The atomic detail of an evaporating meniscus

Jonathan B. Freund
Theoretical and Applied Mechanics, University of Illinois at Urbana-Champaign, Urbana, Illinois 61801

(Received 12 July 2004; accepted 11 November 2004; published online 11 January 2005)

Atomistic simulations of a simple Lennard-Jones fluid are used to investigate the very near-wall dynamics and thermodynamics of evaporating menisci. The specific configuration considered is a two-dimensional (in the mean) liquid drop centered on a cold spot on an atomically smooth solid wall with evaporating menisci extending from it onto hotter regions of the wall. In the four cases simulated, the interaction energy between the solid atoms, which make up the wall, and the fluid atoms, which are equilibrated in liquid and vapor phases, is varied by a factor of about 5. Results are interpreted in the context of a recently proposed continuum model [V. S. Ajaev and G. M. Homsy, "Steady vapor bubbles in rectangular microchannels," J. Colloid. Interface Sci. **240**, 259 (2001)], which is based on a low-capillary-number asymptotic analysis of the flow and heat equations. In this model, the nonlocal influence of the wall is modeled by a disjoining pressure, a common linearized nonequilibrium model is assumed for evaporation kinetics, and the interface curvature impacts thermodynamics through its effect on the local pressure. However, this model and others like it neglect both the atomic granularity of the fluid and any scale associated changes in its properties in the thinnest regions of the evaporating meniscus, which are the subject of this study. Quantitative agreement for meniscus shape and evaporative mass flux is found for a weakly wetting case, but the model must be modified in a straightforward way for more strongly wetting cases to account for a layer of nearly fixed fluid atoms on the wall. A finite solid-liquid interface thermal (Kapitza) resistance is found to be important, and the continuum model is reformulated accordingly. With an appropriate Kapitza resistance value the reformulation yields accurate predictions using the actual wall temperature as a boundary condition, rather than the fluid's temperature at the wall. [DOI: 10.1063/1.1843871]

I. BACKGROUND

The dynamics and thermodynamics of evaporating menisci are central in applications such as nucleate boiling,[1] the growth of vapor bubbles in small fluidic applications (e.g., inkjet printers, optical switches, and others[2]), and in heat pipes.[3] For these, perhaps the most challenging part of the evaporating meniscus to model is its thinnest regions near the solid-liquid-vapor trijunction, where the evaporative mass flux is thought to be high due to the small thermal resistance of the thin liquid film. For instance, nucleate boiling models and experiments suggest that a significant fraction of the overall mass flux into the bubble comes from the microlayer region.[1,4]

Several length-scale associated factors are thought to influence the heat and mass flow near the triphase junction. It is thought that the locally high interface curvature may significantly alter evaporation kinetics through its influence on pressure and that the finite length-scale atomic attraction between the fluid and solid effectively raise the pressure in fluid films on the wall, altering in this case both its dynamics and thermodynamics. This later effect is often modeled by a disjoining pressure, which is proportional to the interaction energy between the fluid and solid atoms and the inverse third power of the film thickness. Wayner[3] provides a thorough review of these effects in the context of evaporating menisci. Taking curvature and disjoining pressure together gives the pressure difference between the liquid and vapor phases as

$$p_v^* - p^* = \frac{\overline{A}}{h^{*3}} + \gamma C, \tag{1}$$

where p_v^* and p^* are the dimensional liquid and vapor pressures, respectively, $6\pi\overline{A}$ is the Hamaker constant for the particular solid and liquid, h^* is the dimensional local thickness of the liquid layer, C is the local interface curvature, and γ is, of course, the surface tension.

The pressure in the liquid film couples into its hydrodynamics, but it also affects evaporation. After Schrage,[5] Schoenberg *et al.*[6] and Ajaev and Homsy[7] model the evaporative mass flux as being linearly proportional to the deviation of the actual vapor pressure from the equilibrium vapor pressure, which in turn depends upon the pressure and temperature jumps across the interface. Employing the notation of Ajaev and Homsy[7] as we do throughout, this yields a mass flux,

$$J = \frac{\delta(p - p_v) + T_i - 1}{K}, \tag{2}$$

which is nondimensionalized by the liquid density ρ and velocity scale U so that $J = J^*/\rho U$. A standard capillary scaling is used to nondimensionalize pressure $p^* = \gamma p/d$, where d is an appropriate macroscopic length scale of the configuration. The dimensional interface temperature and all other temperatures are normalized by the saturated vapor temperature as $T_i = T_i^*/T_s^*$. The constants K and δ in (2) are

$$K = \frac{\rho U \sqrt{2\pi R T_s^*}}{2\rho_v \mathcal{L}}, \quad \text{and } \delta = \frac{\gamma}{\rho \mathcal{L} d}, \tag{3}$$

where $\mathcal{L}$ is the mass specific latent heat of vaporization, ρ_v is the vapor density, and R is the mass specific gas constant. We follow Ajaev and Homsy[7] and take

$$U = \frac{kT_s^*}{\rho \mathcal{L} d} \tag{4}$$

as our velocity scale, with k the thermal conductivity of the liquid. We considered several other possible velocity scales that could be extracted from our atomistic simulations, but this one is unambiguous, is similar in magnitude to other possible choices, and facilitates comparison with their specific formulation. It reflects a balance of energy at the interface.

Appropriate boundary conditions at the wall are no-slip, no penetration, and specified temperature:

$$u^*(x, y=0) = 0, \quad v^*(x, y=0) = 0, \quad T^*(x, y=0) = T_w(x). \tag{5}$$

Neglecting dynamics in the gas phase provides a simple stress boundary condition at the $y=h$ interface. The liquid temperature at the $y=h$ liquid-vapor interface is $T(h)=T_i$. Assuming a low Reynolds number and rescaling dimensions and lengths, velocities, and J and K for small capillary number Ca as

$$x^* = d\mathrm{Ca}^{1/6}\hat{x}, \quad y^* = d\mathrm{Ca}^{1/3}\hat{y}, \quad h^* = d\mathrm{Ca}^{1/3}\hat{h}, \tag{6}$$

$$u^* = U\mathrm{Ca}^{-1/2}\hat{u}, \quad v^* = U\mathrm{Ca}^{-1/3}\hat{v}, \tag{7}$$

$$J = \mathrm{Ca}^{-1/3}\hat{J}, \quad K = \mathrm{Ca}^{1/3}\hat{K}, \tag{8}$$

and retaining only the lowest-order terms in Ca allows the incompressible flow and heat equations to be reduced to an ordinary differential equation for the film thickness,

$$\frac{1}{3}\left[\left(\hat{h}_{\hat{x}\hat{x}} + \frac{\epsilon}{\hat{h}^3}\right)\hat{h}^3\right]_{\hat{x}} + \hat{J} = 0, \tag{9}$$

where the scaled phase-change mass flux is

$$\hat{J} = \frac{T_w(\hat{x}) - 1 - \delta\left(\hat{h}_{\hat{x}\hat{x}} + \dfrac{\epsilon}{\hat{h}^3}\right)}{\hat{K} + \hat{h}}. \tag{10}$$

The group of terms $\hat{h}_{\hat{x}\hat{x}} + \epsilon/\hat{h}^3$ is the pressure relative to p_v according to (1), which appears in (9) as a hydrodynamic factor and in (10) through its thermodynamic influence on the evaporation. The $\epsilon/\hat{h}^3$ term is the disjoining contribution to the pressure with

$$\epsilon = \frac{\overline{A}}{\rho d^2 \mathrm{Ca}}, \tag{11}$$

which has been scaled by Ca to properly retain its influence in the small capillary number limit. Full details of the derivation are provided clearly by Ajaev *et al.*[8] and not repeated here. The only difference at all with their result is a slow variation in the wall temperature $T_w(\hat{x})$, which is needed to match our simulated configuration. The primary assumptions in the derivation can be summarized as (1) constant fluid properties $(\rho, k, \mu, \mathcal{L}, \gamma)$, (2) low Reynolds and capillary numbers (i.e., the lubrication limit with $|u| \gg |v|$ and large scales in x relative to y), (3) neglect of vapor-phase dynamics, (4) a linear nonequilibrium kinetic model of evaporation, (5) a Hamaker-constant disjoining-pressure model for the nonlocal influence of the solid wall, and (6) standard wall velocity and temperature boundary conditions.

In formulating the above model, the atomic granularity of the fluid has been neglected, but may become important in the regions nearest to the wall where the film is atomically thin, a possibility that appears to be well appreciated by Wayner and co-workers[3,6] and Ajaev and Homsy[7] and others[4] who have employed this or similar models. While there is no question that the above formulation is at the very least an appropriate physics based regularization of the flow and heat equations near the triphase line, we can anticipate several ways in which the molecular detail of the system might manifest itself. For one, the small length scales might lead to a local changes in fluid properties. It is known, for example, that extreme confinement can alter the effective viscosity of even the simplest fluids.[9] It is also possible that a single Hamaker-constant disjoining-pressure model of the wall interactions might not be flexible enough to accommodate the actual wall-fluid interactions. In addition, given the thickness of the liquid film, we can anticipate that even a small boundary thermal resistance (Kapitza resistance) might significantly impact the heat and mass transfer.

Checking the quantitative correctness of the continuum model in the thinnest regions of the meniscus is the objective of this paper. The atomic simulation model is discussed in the Sec. II. This in turn is followed by two short sections discussing observations of the atomistic simulations relevant to comparison with (9): Sec. III discusses how wall temperature was maintained and documents the observed temperature jump between the solid and liquid in some cases, and Sec. IV establishes a region of the atomistic simulation model where the lubrication approximation used above should be reasonable. The central result of the paper is the direct comparison of the atomistic simulations with numerical solutions of (9) presented in Sec. V. A correction to (9) for finite Kapitza resistance is formulated and evaluated against the atomistic simulations in Sec. VI.

II. ATOMISTIC SIMULATIONS

Our model atomic system is constructed entirely from Lennard-Jones atoms, which interact via the truncated and shifted Lennard-Jones pair potential,

$$u(r) = \begin{cases} u_{LJ}(r) - u_{LJ}(r_c), & \text{if } r \leqslant r_c, \\ 0, & \text{if } r > r_c, \end{cases} \tag{12}$$

where u_{LJ} is the standard Lennard-Jones 6-12 pair potential,

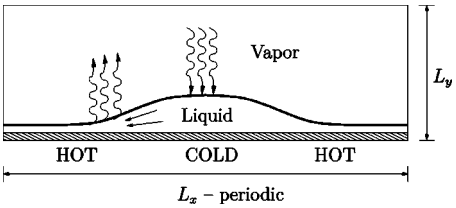

FIG. 1. Schematic of atomistic simulation configuration.

$$u_{LJ}(r) = 4\varepsilon_{ij}\left[\left(\frac{\sigma_{ij}}{r}\right)^{12} - \left(\frac{\sigma_{ij}}{r}\right)^{6}\right]. \tag{13}$$

This atomic model is, of course, limited in the range of real materials that it can represent accurately, though it is commonly used for studies of atomic phenomena. We select it here for the speed with which it can be computed and because the properties of Lennard-Jones fluids and solids are well documented, allowing us to use some physical parameters available in the literature in the continuum model. We see it as an appropriate first step in understanding the phenomenological influence of realistic atomic granularity on the evaporating meniscus system.

In (13), the energy of an interaction between atoms of type i and j is ε_{ij} and the Lennard-Jones length scale of this interaction is σ_{ij}, which corresponds to a zero-force radius of $r_o = 2^{1/6}\sigma_{ij}$. All atomic interactions in all the simulations discussed in this paper have the same $\sigma_{ij} = \sigma$. A finite cutoff radius $r_c = 2.5\sigma$ was selected in (13) to reduce the number of interactions that needed to be evaluated in order to speed the computations. The impact of this choice on r_c-sensitive properties such as the surface tension is discussed in Sec. V.

The equation of motion was integrated in time using the second-order simplectic velocity-Verlet algorithm with a numerical time step of $\Delta t^\dagger = 0.0046$. Throughout, a superscript † indicates quantities that are nondimensionalized by the Boltzmann constant and the mass and Lennard-Jones parameters of the fluid atoms: k_B, m_f, ε_{ff}, and σ.

Though all standard methods to accelerate the numerical solution were applied, it is computationally impractical to simulate the growth of a three-dimensional vapor bubble on a hot wall or similar full-system representations of the other target applications discussed in Sec. I. So, instead, we have designed a model system that is both tractable for atomistic simulation and can be compared directly with (9). The geometry of the selected configuration is shown schematically in Fig. 1. A liquid drop sits on a cold spot on an atomically smooth solid wall with its meniscus extending onto hotter regions of the wall. The liquid flows into these hot meniscus regions and evaporates. To maintain the thermodynamic equilibrium of the entire finite-volume system, vapor condenses on the cold top of the drop. The resulting flow is statistically stationary, allowing us to average in time to converge statistics.

Periodic boundary conditions were applied in all three coordinate directions. The dimensions of the simulated system are $L_x^\dagger = 205$ parallel to the wall temperature gradient and $L_y^\dagger = 58.7$ perpendicular to the wall. To further reduce the number of atoms required, the drop is constrained by the size of the computational box to be two dimensional in the mean. The system is homogeneous in the out-of-the-page z direction with a domain that extends $L_z^\dagger = 6.35$. We take $x^\dagger = 0$ to be the middle of the drop and $y^\dagger = 0$ to be the mean position of the topmost wall atoms plus $2^{1/6}/2\sqrt{2}$, which is expressed in the seemingly awkward form to show explicitly that this distance is half way to the y location of the where the next wall atom would sit on the exposed (010) surface of the fcc lattice. Since the wall and fluid atoms have the same σ, this will also, therefore, be about half the vertical distance to where the first fluid atom could sit on the wall.

The atoms in the wall have $m_s = 10m_f$ and $\varepsilon_{ss} = 10\varepsilon_{ff}$, which were set to give this material a high melting temperature and make it stiff without imposing a fast vibrational time scale on the simulations. The 6192 solid atoms were initially positioned in five layers (2.5 unit cells) of a fcc lattice, the bottom layer of which was held fixed to maintain the integrity of the wall. This bottom layer was also different in that its interaction with the fluid atoms had an energy of only $0.01\varepsilon_{ff}$. This was selected to prevent another drop condensing on the bottom side of the solid, which would otherwise happen given the periodic boundary conditions. The 7420 fluid atoms were also initialized in a fcc lattice, but in this case in the shape of a semicircle sitting on the wall and centered in the anticipated drop location. At the beginning of the simulations, these atoms immediately melt and spread and some evaporate.

The total potential energy and mean temperature were monitored to track the evolution of the system and establish when it became statistically stationary, which was achieved in the first 3×10^6 numerical time steps. Statistics were accumulated over the next $\approx(100-200)\times10^6$ time steps. Density, velocity, and temperature data were collected in an array of 100×100 bins covering the x-y plane. Typically, ensembles with different random initial velocities were simulated and averaged to give the results reported below.

Four cases with different $\varepsilon_{sf} = E_r\varepsilon_{ff}$ are reported in this paper: $E_r = 0.75$, 1.0, 2.0, and 4.0. By assuming that interface energies depend only upon the interaction energies of the constituent atoms and neglecting interactions with the gas phase, we can anticipate a contact angle of

$$\theta \approx \cos^{-1}(2E_r - 1) \tag{14}$$

from Young's law.[10] This formula neglects the atomic structure of the interfaces, but provides the estimate that in absence of flow and evaporation we would have $\theta = 60°$ for the $E_r = 0.75$ case. The other cases are all wetting. We found previously that this formula for θ reasonably predicted a $\theta = 83°$ contact angle in a similar but isothermal configuration.[11] Of course, in the present case, the hydrodynamics coupled to the mass transfer along with the thermodynamics will affect the shape of the drop.

III. WALL TEMPERATURE

Wall temperature $T_w(x)$ was maintained with the thermostat proposed by Anderson.[12] In this approach, each step in the numerical time integration there is a finite probability for each atom in the thermostated region to be assigned a new

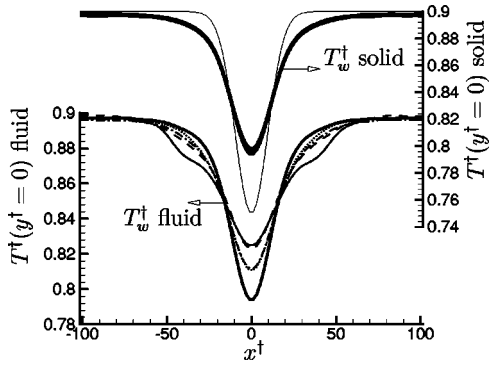

FIG. 2. Wall temperature. The *top* set of curves show the temperature in the solid at the wall for all four cases (—). The thin solid (—) line shows the thermostat target temperature (15). The *bottom* set of curves shows the wall temperature in the fluid phase: —, $E_r=0.75$; ----, $E_r=1.0$; -·-, $E_r=2.0$; and ·····, $E_r=4.0$. The heavy (—) line is the solid-phase T_w for the $E_r=0.75$ case and is shown for reference. The atomistic temperature data were smoothed for plotting clarity by retaining the first ten terms of the cosine series representation of the data.

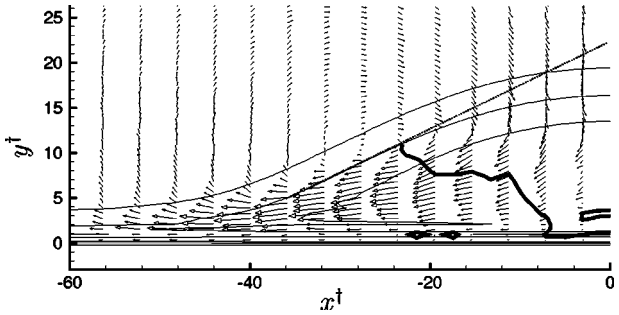

FIG. 3. The arrows show the local mass flux vector $\rho\mathbf{u}$, the thin contours (—) show the 10%, 50%, and 90% points between the liquid and vapor density, and the (—) line indicates where the magnitude of the velocity vector angle is 20° (see text). The hand placed (·····) line is inclined at 25°.

velocity randomly selected from an appropriate Boltzmann distribution. The advantage of this over a more common velocity rescaling approach is that it does not require an estimate of the current temperature of the region to be thermostated. Like any thermostat[13] it does alter the atomic dynamics to some degree and hence the physical properties of the material, but only for the solid-wall atoms where it is applied and not of the fluid atoms whose behavior is our focus. The target wall temperature was

$$T_w^\dagger(x^\dagger) = T_h^\dagger + (T_c^\dagger - T_h^\dagger)e^{-(x^\dagger/s^\dagger)^2} \tag{15}$$

with $T_h^\dagger=0.9$, $T_c^\dagger=0.75$, and $s^\dagger=13.7$. However, the thermostat was set to be relatively weak with probability of velocity reassignment $\nu=0.001$ to minimize its impact on the dynamics, so the wall temperature was able to deviate from this profile somewhat because of heat conduction within the wall and to the fluid above it. The top set of curves in Fig. 2 shows the target and observed wall temperatures, whereas the bottom set of curves shows the temperature of the fluid atoms closest to the wall. We see that there is a jump in temperature between the solid and the liquid that depends upon E_r. The smaller the solid-fluid interaction energy (smaller E_r), the larger the temperature jump is. This trend is consistent with recent atomistic simulations of the Kapitza resistance of Lennard-Jones solid-fluid systems.[14] In Sec. V, where we make a direct comparison of solutions of (9) with the atomistic results, we take the fluid temperature at the wall (the bottom curves in the figure) and not the actual wall temperature to be our $T_w(x)$ in (10). This provides the most direct evaluation of (9) and (10), since it is most consistent with the original assumptions leading to this formulation. In Sec. VI, we revisit the actual wall temperature and modify (10) to accommodate a finite Kapitza resistance.

IV. LUBRICATION APPROXIMATION

Before we compare the atomistic simulation results to (9), we need to first identify a region where the lubrication approximation is sufficiently well satisfied to make the comparison fair in this regard. Figure 3 shows the position and location of the drop with contours of mean density. Depending somewhat on the specific size definition of the drop's extent, its height to half-width (from center to edge) ratio is $\approx 3:8$ in all cases. While this is not obviously small enough, the lubrication approximation is known to be robust and we shall see quite remarkable agreement in the following at least for interface slope and evaporation. The liquid wedge angle estimated with the hand placed dotted line in the figure is $\approx 25°$. The thick contour marks the $|\alpha|=20°$ condition in the liquid region defined for now to have density $\rho > (\rho_v+\rho_l)/2$, where $\alpha=\tan^{-1}v/u$ is the angle of the velocity vector $\mathbf{u}=(u,v)$. So, while we will certainly be violating any strict asymptotic limit, there is hope given the robustness of the lubrication approximation for favorable agreement when $|x^\dagger| \gtrsim 30$. Reynolds numbers based on observed local peak velocities and liquid-film thicknesses are $\lesssim 0.025$.

V. DIRECT COMPARISON WITH EQ. (9)

A. Physical parameters

The several parameters that must be specified in making a direct evaluation of the asymptotic theory presented in Sec. I are given in Table I. Some are deduced directly from the simulations, while others have been taken from documented properties of Lennard-Jones fluids. The latent heat of vaporization was deduced from an accepted value for argon, which is known to be well modeled by a Lennard-Jones potential. Additional details concerning the selected values are provided as footnotes to the table.

One parameter that requires additional discussion is the surface tension γ. More than any of the other parameters, surface tension is known to be sensitive to the truncation length of the interatomic potential, and for Lennard-Jones fluids it is known to increase significantly with r_c for values up to $r_c^\dagger \approx 6.5$.[15,16] However, since the computational expense scales as r_c^3, using $r_c^\dagger=6.5$ would restrict the scope of this investigation. Fortunately, Lennard-Jones fluids simulated with $r_c^\dagger=2.5$ do have a well defined γ, although it is approximately one half of the accepted $r_c\to\infty$ value. So we simply use this $r_c^\dagger=2.5$ surface tension value (Table I) in making our comparison. Finite r_c should also affect the Hamaker con-

TABLE I. Physical parameters for comparison with (9).

Parameter	Value	Source
$\rho^\dagger$	0.70	Mean in bulk liquid[a]
$\mu^\dagger$	1.20	Lennard-Jones simulation data fit of Rowley and Painter[b]
$\gamma^\dagger$	0.24	Interpolated from Table II of Trokhymchuk and Alejandre[c]
$k^\dagger$	4.79	Extrapolated from simulation data of Borgelt *et al.*[d]
$\mathcal{L}^\dagger$	6.52	Deduced from argon latent heat of 6.5 kJ/mole
$\rho_v^\dagger$	0.034	Mean in vapor on $y^\dagger=50$ line[e]
$T_s^\dagger$	0.87	At the vapor stagnation point at $x^\dagger=0$ and $y^\dagger\approx 50$

[a]The density varies continuously through the drop due to temperature variation, but for the $E_r=1$ drop, as an example, it varied by less than 1% from this value for $y^* \in [5,13]$ and $x^* \in [-15,15]$.
[b]It should be noted that Rowley and Painter's (Ref. 19) cutoff radius was $r_c=4.0\sigma$, rather than the $r_c=2.5\sigma$ in the present work. Also, the coefficient misprints in that paper were corrected as indicated by Zabaloy *et al.* (Ref. 20).
[c]The interface temperature is observed to vary by less than 4% over the entire drop, so neglect of Maragoni effects appears justified. The value used is for the mean T_i in region of comparison. Reference 15.
[d]Corresponds to 0.09 W/m K for argon. Reference 21.
[e]Variation of the mean vapor density is less than 1% from this value at $y^\dagger=50$.

stant and thus the disjoining pressure, but we present evidence in Sec. V C. suggesting that it is unimportant in the present case.

B. Interface definition

Since there is no obvious specific phase boundary in the atomistic simulation, we must designate one for making our comparisons. At the interface, the time average of the thermal motions of the phase boundary lead to continuous transition between liquid and vapor phases over several atomic dimensions. This is seen in Fig. 3, where mean density changes smoothly between its values in the liquid and vapor phases such that the 10% and 90% density points are approximately $\approx 6\sigma$ apart. The apparent interface thickness is thus thicker than the apparent attached film thickness over the hot regions of the wall, so the choice of a single interface location $h(x)$ within this finite thickness is important. We use an equivalent-mass definition. At each x location we define an equivalent bulk-liquid-density film thickness as

$$h(x)=\frac{\int_0^H \rho(y)dy - H\rho_v}{\rho_l-\rho_v}, \tag{16}$$

where $\rho(y)$, ρ_l, and ρ_v are the local density, the bulk liquid density and the bulk vapor density, respectively. This film thickness, whose independence of H for large enough H was verified directly, is the thickness of an equivalent mass (per unit dimension in y and z) liquid film having constant density ρ_l. Near the top of the drop, where the transition between liquid and vapor phases is nearly symmetric about the $\rho=(\rho_l+\rho_v)/2$ isopleth, this measure well approximates this 50% density contour.

TABLE II. Corrections from $\bar{A}_o$ defined in Eq. (17) to match hot-wall film thickness by Eq. (18).

E_r	h_o	H_r
0.75	0.380	0.007
1.0	1.597	0.424
2.0	1.954	0.366
4.0	2.433	0.362

While (16) is an appropriate thickness for comparing with (9) predictions, computing the evaporative flux at this $h(x)$ would lead to errors because, as we shall see, a significant portion of the flow in the film is in the diffuse layer above the $h(x)$ selected according to (16). So, when computing J, we use the $\rho_c=0.2\rho_l$ contour to define the location of the interface $y=h_c$. We observe J to change by only a few percent when a ρ_c criterion even closer to ρ_v is used. The flux is then computed directly as $J=\rho(h_c)u_n(h_c)$, which is the local density multiplied by the local interface normal velocity. While selecting h_c such that $\rho(h_c)$ is closer to ρ_v would presumably capture a little more evaporation (we observe $\lesssim 3\%$), it has the drawback of smoothing the evaporation flux profile. That is, for smaller ρ_c, the sharp peaks observed in the $J(x)$ profile are smoothed out because they are further from where most of the phase change occurs. Hence we take $\rho_c=0.2\rho_l$ as a compromise between computing every bit of $J(x)$ and identifying precisely where the evaporation occurs.

C. Hamaker constant

A final parameter, not listed in Table I, which needs to be discussed before making our comparisons is the reduced Hamaker constant $\bar{A}$, which appears in (9) in nondimensional form through ϵ defined in (11). A crude estimate of $\bar{A}$ in terms of the atomic interaction energies is[17]

$$\bar{A}_o=\tfrac{2}{3}\pi\varepsilon_{sf}\sigma^6 n_s n_f, \tag{17}$$

where n_s and n_f are the number densities of the solid and fluid atoms, respectively. Like (14), this simple estimate neglects details concerning the arrangement of the atoms. The nondimensional Hamaker factor ϵ appears in two places in (9) and (10), but its most obvious impact on the solution is the equilibrium film thickness on the hot portion of the wall. Assuming that the film is flat, (9) and (10) reduce to

$$\hat{h}_o=\sqrt[3]{\frac{\epsilon\delta}{T_w-1}}. \tag{18}$$

We present results only for a corrected $\bar{A}=H_r\bar{A}_o$, where H_r is selected so that (18) matches the observed film thickness according to our definition (16). These H_r values are given in Table II. We see that for the wetting ($E_r \geqslant 1$) cases the H_r correction factor is nearly constant, varying from its mean value by less than 10%, which indicates that our model truncated potential (12) with $r_c^\dagger=2.5$ is acceptable, at least as far as our definition of film thickness is concerned. The values might be somewhat sensitive to r_c, but the trend is as expected, which is more important for our objectives. Also

noteworthy in the wetting cases is that H_r is reasonably close to unity, indicating that (17) provides a not-too-bad value for the Hamaker constant, perhaps underestimating the best value for matching the $\hat{h}_o$ thickness because of the small r_c used, just as finite r_c reduces the effective surface tension. The nonwetting $E_r=0.75$ case is, as might be anticipated, anomalous. Its effective film thickness is only about one third the atomic dimension, so it cannot be expected to behave as a continuum fluid anyhow. In the following, we use Table II values of H_r in solving (9). Using the mean value of the $E_r \geqslant 1$ cases would have little impact on the solution, especially given the cube-root dependence of $\hat{h}_o$ on ϵ. Using $\overline{A_o}$ does noticeably change the results, but since this is an easily studied property of (9), we do not explore this. We take this course because our objective is to best evaluate (9) assuming that good estimates of all the physical parameters are available, though in the end the Hamaker constant might be the most challenging to obtain in practice.

D. Comparison

We solved (9) on $\hat{x} \in [a,b]$, where a is the left edge of the atomistic simulation domain and b is the point on the drop where the lubrication approximation is deemed reasonable as discussed in Sec. IV. Appropriate boundary conditions are thus

$$\hat{h}_{\hat{x}}(a)=0, \quad \hat{h}_{\hat{x}\hat{x}\hat{x}}(a)=0, \quad \hat{h}_{\hat{x}}(b)=\hat{s}_o, \quad \hat{h}_{\hat{x}\hat{x}}(b)=\kappa_o, \quad (19)$$

where the conditions at a reflect the symmetry at the periodic boundary and the conditions at b are the appropriately scaled slope and curvature taken from the atomistic simulation. The correct film thickness on the hot wall far from the drop is guaranteed by our choice of H_r. Since there is no macroscopic length scale d in our model flow, it was selected for our evaluation so that $\hat{h}(b)$ also matched the atomistic simulation results. Capillary numbers based on (4) with $d=L_x$, the largest length in the model flow, would be small with Ca $\lesssim 0.005$, though any truly macroscopic length scale for d would make this much smaller still.

Equation (9) with flux (10) was solved by time marching its unsteady analog[8] to a steady state using an implicit time advancement algorithm and spectral matrix collocation with Chebyshev polynomial basis functions. Parts (a) of Figs. 4–7 show comparisons of the atomistic and Eq. (9) interface profiles. Perhaps not too surprisingly given the simplicity of the interface shape and the number of conditions specified at the boundaries, agreement is seen to be good.

The mass fluxes in part (b) of these figures, however, show a very different behavior than might be anticipated given the apparent success at predicting the surface shape. It would probably not be too surprising if the nonwetting $E_r=0.75$ case deviated significantly from the continuum model in Fig. 4(b) because the wall film in this case is significantly thinner than the atomic dimension. Still, (9) does provide a reasonable prediction for the mass flux, especially if what is sought is an appropriate regularization for the neighborhood of the trijunction.

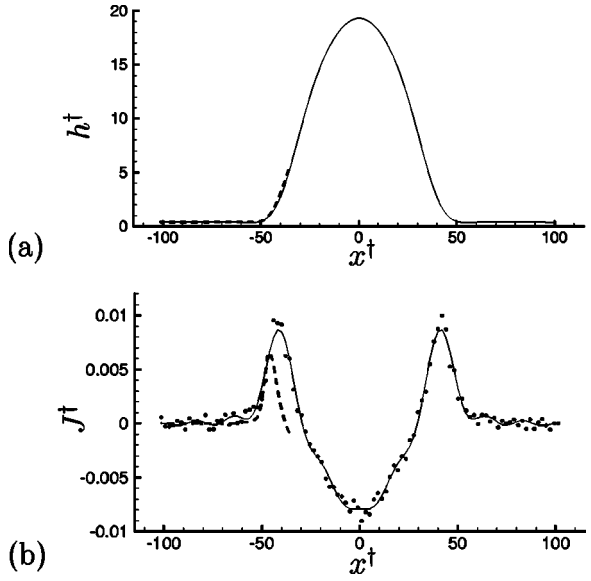

FIG. 4. Case $E_r=0.75$: (a) The Eq. (16) film thickness for the atomistic simulation (—) and Eq. (9) (----); (b) $J^\dagger$ for the atomistic simulation (●) with Fourier smoothed fit (—) and Eq. (10) prediction (----).

Better agreement is expected for the wetting cases, and indeed the $E_r=1.0$ mass flux shown in Fig. 5(b) is remarkably close to the prediction. However, for the $E_r=2.0$ and $E_r=4.0$ cases shown in Figs. 6(b) and 7(b) the predicted mass flux, having matched the interface shape, becomes progressively worse, falling well below that of the atomistic simulation in the $E_r=4.0$ case. This is particularly surprising, since the theory presented in Sec. I predicts that the net evaporative flux in the meniscus should increase as a function of ϵ, all other things being equal. The atomistic simulations for the wetting cases all have nearly the same net J as shown in Fig. 8. The particular rescalings and boundary con-

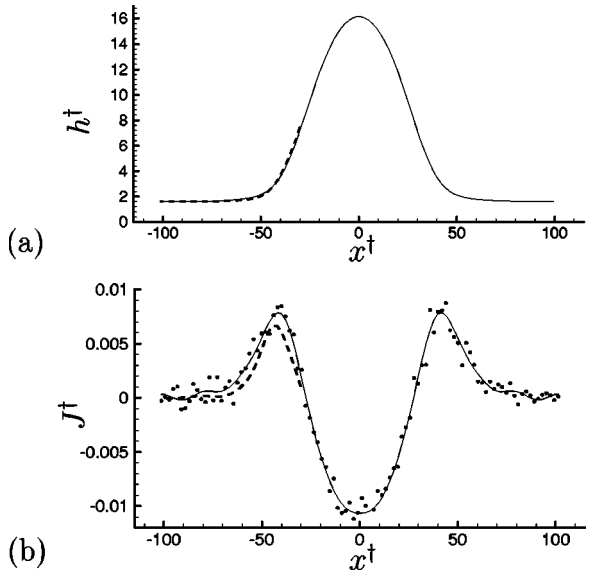

FIG. 5. Case $E_r=1$: (a) The Eq. (16) film thickness for the atomistic simulation (—) and Eq. (9) prediction (----); (b) $J^\dagger$ for the atomistic simulation (●) with Fourier smoothed fit (—) and Eq. (10) prediction (----).

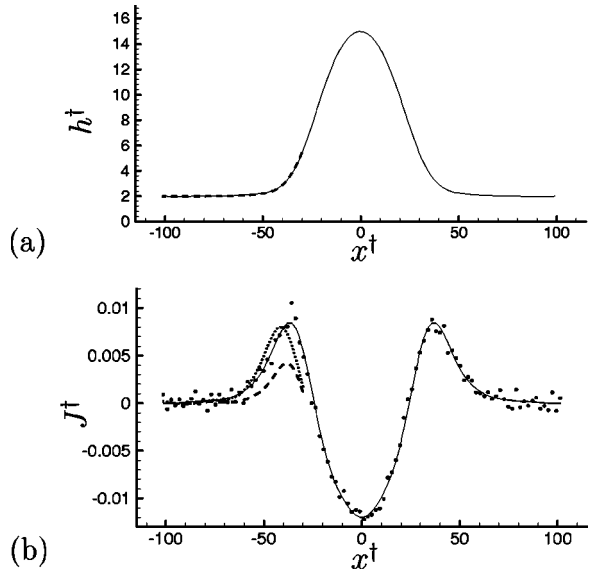

FIG. 6. Case $E_r=2$: (a) The Eq. (16) film thickness for the atomistic simulation (—) and Eq. (9) prediction (----); (b) $J^\dagger$ for the atomistic simulation (●) with Fourier smoothed fit (—), the Eq. (10) prediction (----), and the Eq. (10) prediction with effective wall location correction (·····) (see text).

ditions that match interface shapes at the boundaries, however, clearly yield a contradictory behavior for the net J.

The reason for this discrepancy seems to be that the fluid atoms in the thinnest regions of the meniscus resist flow much more than the constant Newtonian viscosity continuum model assumes. Less flow toward the hotter regions of the surface corresponds to less evaporation from that region. Figure 9, which shows mass flux vectors for all four cases, suggests that for the $E_r=2.0$ and $E_r=4.0$ cases the atoms closest to the wall are effectively fixed in place (in the mean), not flowing at all. It is well known that a wall induced ordering can occur locally in liquids,[18] but in this case

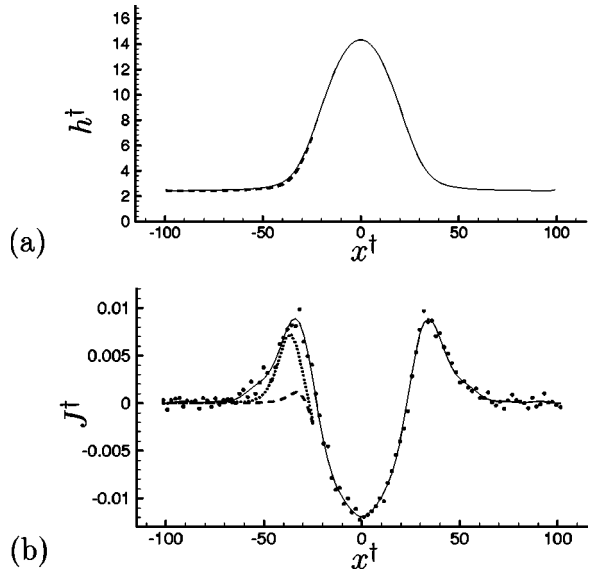

FIG. 7. Case $E_r=4$: (a) The Eq. (16) film thickness for the atomistic simulation (—) and Eq. (9) ---- prediction; (b) $J^\dagger$ for the atomistic simulation (●) with Fourier smoothed fit (—), the Eq. (10) prediction (----), and the Eq. (10) prediction with effective wall location correction (·····) (see text).

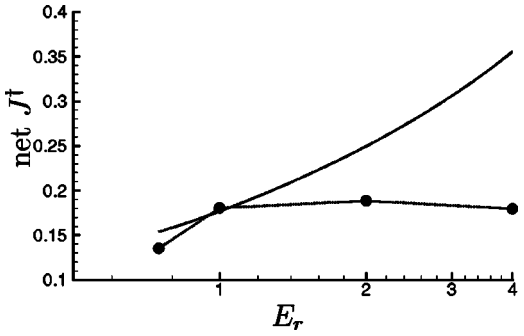

FIG. 8. Total evaporative (positive) $J^\dagger$: (—) solved via (9) with parameters other than ϵ matching the $E_r=1.0$ case; (●) atomistic simulations.

the atoms in these apparently quasicrystalline regions next to the wall do not flow. We should note, however, that the details of this observation may be sensitive to the $\sigma=\sigma_{ss}=\sigma_{sf}=\sigma_{ff}$ of the present study, which might facilitate this apparent

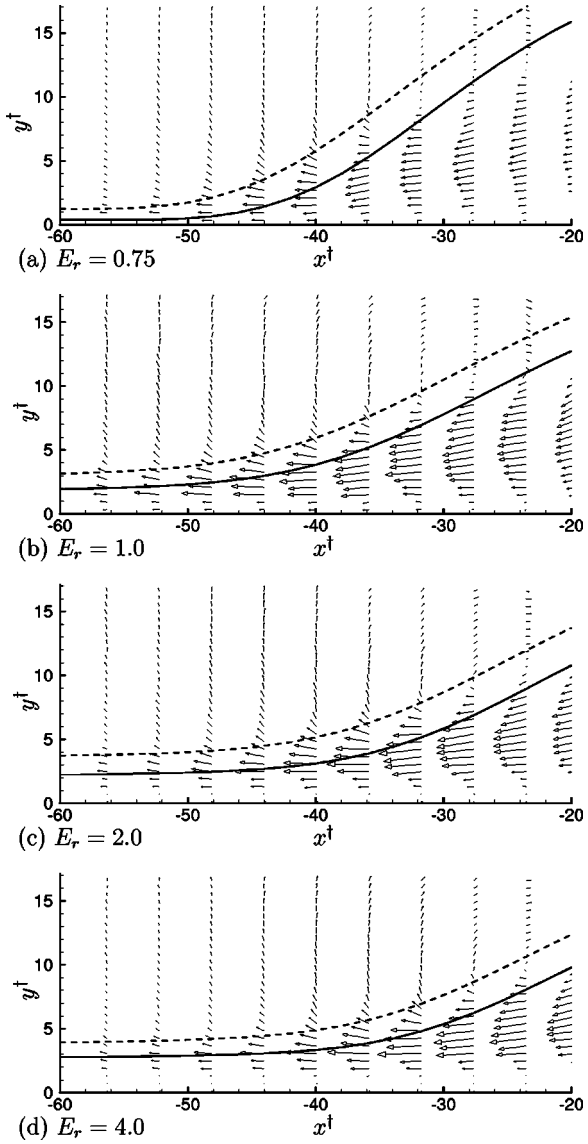

FIG. 9. The arrows show the local mean mass flux $\rho\mathbf{u}$ and the solid (—) lines show the liquid-vapor interfaces as defined in (16). The dashed (----) lines indicate the $\rho_c=0.2\rho_l$ isopleth where we compute J.

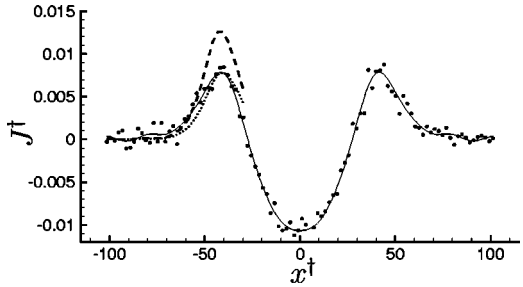

FIG. 10. Evaporative flux using the $y=0$ temperature of the solid: (—) atomistic simulation, (----) Eq. (9) with (10) for mass flux, and (·····) Eq. (9) with (22) for the mass flux with $\ell^\dagger=4.0$.

solidification of the near-wall fluid atoms.

If we treat these stuck fluid atoms as solid-wall atoms by shifting the y coordinate so that the no-slip boundary condition is applied at the appropriate point within the nominally liquid layer, the agreement with the continuum model is again excellent. The dotted ····· line in Fig. 6(b) shows the $E_r=2.0$ case, but now with $y^\dagger=0$ shifted upward by 0.7 as suggested by Fig. 9(c) and a new H_r used to match the new effective film thickness on the hot wall. Both the interface shape (not shown) and the J profile match the atomistic data well. Likewise, when the $E_r=4.0$ case is shifted upward by 1.2 in $y^\dagger$, the agreement is also very good, as seen with the dotted line ····· in Fig. 7(b). Fine tuning the $y^\dagger=0$ point could presumably further improve the agreement.

Oftentimes, meniscus flows are regularized in their continuum description by the introduction of velocity slip at the wall, with a slip length defined as the effective location of the no-slip condition within the wall assuming a linear extrapolation of the near-wall velocity. Our upward shift of the effective wall location amounts in effect to the imposition of a negative slip length, presumably brought on physically by a complex viscoplastic and/or viscoelastic local rheology. A detailed study of this is warranted, but is beyond the scope of this effort.

VI. KAPITZA RESISTANCE

As discussed in Sec. III, the temperature in the atomistic simulations is observed to jump discontinuously between the top wall atoms and the fluid atoms closest to the wall. This indicates that there is a finite Kapitza resistance R_K at the solid-fluid interface. To include this in the analysis, it is convenient to define a Kapitza length $\ell^* \equiv R_K k$, which is the effective thickness of a layer of liquid that would have the same thermal resistance as the solid-liquid boundary. It is analogous to the slip length commonly defined for slipping velocity boundary conditions. Typical ℓ^*'s are only a few atomic spacings, making this boundary resistance negligible at macroscopic scale but possibly important for the thinnest meniscus films. Indeed, using the actual T_w of the solid and repeating the calculation in Fig. 5 with the same $T(y=0)=T_w$ boundary condition gives a significantly too large heat flux, as seen in Fig. 10.

For finite ℓ^*, the wall temperature boundary condition is

$$\frac{\partial T^*}{\partial y^*} = \frac{1}{\ell^*}(T^* - T_w^*), \tag{20}$$

which upon rescaling ℓ^* consistently as $\ell^* = \ell d \mathrm{Ca}^{1/3}$ gives

$$T_{\hat{y}} = \frac{1}{\hat{\ell}}(T - T_w). \tag{21}$$

With this boundary condition, it is a lengthy but straightforward procedure to redo the Ajaev *et al.*[8] derivation, which yields a simple addition of ℓ to the denominator of the mass flux in (10),

$$\hat{J} = \frac{T_w(\hat{x}) - 1 - \delta\left(\hat{h}_{\hat{x}\hat{x}} + \dfrac{\varepsilon}{\hat{h}^3}\right)}{\hat{K} + \hat{h} + \hat{\ell}}. \tag{22}$$

Thus, we see that the Kapitza resistance acts in series with what can be considered the evaporative resistance $\hat{K}$ and the thermal resistance of the liquid film of thickness $\hat{h}$.

The Kapitza resistance at a Lennard-Jones fluid-solid interfaces has been recently computed by Barrat and Chiaruttini[14] using atomistic simulation. In that study, the solid atoms had the same mass as the liquid atoms and same interaction energy, but were held in place by weak harmonic springs. Here we have a significantly stiffer solid, but with our correspondingly larger atomic masses the fcc lattice dispersion relations and wave speed, the mismatch of which across a boundary is widely held to be a key factor setting R_K, are similar to those in the study of Barrat *et al.*[14] Taking $\ell^\dagger=4$ as they found for $E_r=1.0$, produces a good approximation of the J from the atomistic simulations, as seen in Fig. 10.

VII. CONCLUSIONS

In summary, we find that the low-Ca theory summarized in Sec. I is remarkably accurate for predicting the interface shape and mass flux of evaporating menisci even down to the atomic dimensions of the wall-bound film. In making comparisons, the continuum model was solved with boundary conditions consistent with the atomistic simulation results. All physical parameters used in the evaluation aside from the Hamaker constant were taken from independent sources or firm estimates. The Hamaker constant, which is perhaps the hardest to obtain precisely in practice, was selected to match the asymptotic film thickness on the hottest regions of the wall. This is, in a sense, equivalent to assigning another boundary condition on the thin-film side of the domain. Still, the best-fit Hamaker constants were just less than half of what a crude estimate would have suggested.

With the wall temperature taken to be that of the fluid atoms closest to the wall, no modification to the theory was found to be necessary in the weakly wetting case ($E_r=1.0$). However, in the more strongly wetting cases it was found that the fluid atoms right on the wall are effectively immobile. In this case, the continuum model was reapplied with the no-slip boundary condition at the approximate y location of the topmost fixed fluid atoms. This simple procedure pro-

vided the same level of agreement as in the weakly wetting case, though it is not thought that in any of the cases that the velocity profile within the film is exactly as predicted by the lubrication model. There was insufficient binning resolution in the film to assess this directly, but since it is only a few atoms across and the liquid has significant density variation due to its quasi-crystalline structure next to the wall, it is not clear that a direct comparison would be meaningful. This correction depends upon the empirically observed thickness of the fixed fluid layer, but the dependence of this on the parameters of the system is unknown.

A finite temperature jump at the wall indicated a significant Kapitza resistance, and using the wall temperature determined in the solid rather than in the fluid at the wall gave poor predictions of the evaporative mass flux. The continuum model was therefore rederived with an appropriate thermal wall boundary condition allowing for finite boundary resistance. Employing a recently reported Kapitza resistance value allowed us to use the actual wall temperature and still closely match atomistic results.

In closing, we should point out that there are numerous phenomena not represented in our model Lennard-Jones systems that might demand additional modification of the continuum model before quantitatively predictions might be possible. Factors like roughness (even with nanometer length scale), more complex fluids, and more complex fluid-solid interactions all might resist parameterization within the theory considered here as far as quantitatively precise predictions are concerned. Still agreement with the continuum model, even for the Lennard-Jones system, is remarkable given that it models flow, heat conduction and phase change in atomically thin layers.

ACKNOWLEDGMENTS

The author is grateful for fruitful discussions about evaporating menisci with V. S. Ajaev, V. Dhir, and S. Shina and for a few pointers on Chebyshev-τ methods provided by R. D. Moser.

[1] V. K. Dhir, "Boiling heat transfer," Annu. Rev. Fluid Mech. **30**, 365 (1998).
[2] L. Lin, A. P. Pisano, and V. P. Carey, "Thermal bubble formation on polysilicon micro resistors," J. Heat Transfer **120**, 735 (1998).
[3] P. C. Wayner, Jr., "Intermolecular forces in phase-change heat transfer: 1998 Kern award review," AIChE J. **45**, 2055 (1999).
[4] D. Qiu, G. Son, V. K. Dhir, D. Chao, and K. Logsdon, "Dynamics of single and multiple bubbles and associated heat transfer in nucleate boiling under low gravity conditions," Ann. N.Y. Acad. Sci. **974**, 378 (2002).
[5] R. W. Schrage, *A Theoretical Study of Interface Mass Transfer* (Columbia University Press, New York, 1953).
[6] J. A. Schonberg, S. DasGupta, and P. C. Wayner, Jr., "An augmented Young-Laplace model of an evaporating meniscus in a microchannel with high heat flux," Exp. Therm. Fluid Sci. **10**, 163 (1995).
[7] V. S. Ajaev and G. M. Homsy, "Steady vapor bubbles in rectangular microchannels," J. Colloid Interface Sci. **240**, 259 (2001).
[8] V. S. Ajaev, G. M. Homsy, and S. J. S. Morris, "Dynamic response of geometrically constrained vapor bubbles," J. Colloid Interface Sci. **254**, 346 (2002).
[9] K. P. Travis and K. E. Gubbins, "Poiseuille flow of Lennard-Jones fluids in narrow slit pores," J. Chem. Phys. **112**, 1984 (2000).
[10] P. G. de Gennes, "Wetting: statics and dynamics," Rev. Mod. Phys. **57**, 827 (1985).
[11] J. B. Freund, "The atomic detail of a wetting/de-wetting flow," Phys. Fluids **15**, L33 (2003).
[12] H. Anderson, "Molecular dynamics at constant pressure and/or temperature," J. Chem. Phys. **72**, 2384 (1980).
[13] D. Frenkel and B. Smit, *Understanding Molecular Simulation* (Academic, New York, 1996).
[14] J.-L. Barrat and F. Chiaruttini, "Kapitza resistance at the liquid solid interface," Mol. Phys. **101**, 1605 (2003).
[15] A. Trokhymchuk and J. Alejandre, "Computer simulations of liquid/vapor interface in Lennard-Jones fluids: Some questions and answers," J. Chem. Phys. **111**, 8510 (1999).
[16] M. Mecke, J. Winkelmann, and J. Fischer, "Molecular dynamics simulation of the liquid-vapor interface: the Lennard-Jones fluid," J. Chem. Phys. **107**, 9264 (1997).
[17] J. Israelachvili, *Intermolecular and Surface Forces* (Academic, New York, 1992).
[18] J. Koplik and J. R. Banavar, "Continuum deductions from molecular hydrodynamics," Annu. Rev. Fluid Mech. **27**, 257 (1995).
[19] R. L. Rowley and M. M. Painter, "Diffusion and viscosity equations of state for a Lennard-Jones fluid obtained from molecular dynamics simulations," Int. J. Thermophys. **18**, 1109 (1997).
[20] M. S. Zabaloy, J. M. V. Machado, and E. A. Macedo, "A study of Lennard-Jones equivalent analytical relationships for modeling viscosities," Int. J. Thermophys. **22**, 829 (2001).
[21] P. Borgelt, C. Hoheisel, and G. Stell, "Exact molecular dynamics and kinetic theory results for thermal transport coefficients of the Lennard-Jones argon fluid in a wide region of states," Phys. Rev. A **42**, 789 (1990).